Engineering Structures 270 (2022) 114855

Contents lists available at ScienceDirect

Engineering Structures

journal homepage: www.elsevier.com/locate/engstruct

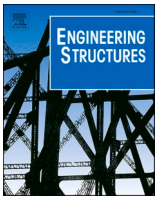

Simulation of impact force generated by an ISO tapping machine on a wooden slab using explicit dynamics analysis

Jesse Lietzén *, Juho Sormunen, Sami Pajunen, Mikko Kylliäinen

Tampere University, Faculty of Built Environment, Unit of Civil Engineering, Korkeakoulunkatu 5, P.O.Box 600 , 33014 Tampere University, Finland

ARTICLE INFO

Keywords:
Impact sound insulation
Impact force
FEM
Explicit time integration
LS-DYNA
Tapping machine
Wooden floor
CLT

ABSTRACT

Application of simulation tools to compute impact sound insulation properties of wooden floors has raised interests in recent decades. To achieve accurate results from the prediction models, information from force excitation generated by impact sound sources is required. The purpose of our study was to present a validated procedure to determine the non-linear impact force excitation generated by an ISO tapping machine. The method comprised use of finite element method (FEM) and explicit time integration to compute impact force pulse generated by a hammer of the tapping machine. With a post-processing procedure, the force pulses can be converted to present point forces describing the continuous operation of the tapping machine on the floor. To demonstrate the applicability of the method, the finite element model was applied to imitate an experimental situation on a cross-laminated timber (CLT) slab. The model validation showed that the computational model closely predicts the force pulse generated on the CLT slab. Findings from a sensitivity analysis revealed that local properties of the slab were the most important to the simulated impact force pulse. The findings of the analysis are helpful for those developing simulation tools to compute the impact force generated by the tapping machine on wooden floors.

1. Introduction

In the recent decades, the use of finite element method (FEM) and other simulation tools to compute impact sound insulation (ISI) of wooden floors has raised interests [1–5]. In a classic description, the prediction models have been divided in three parts: the excitation, the system, and the response. In this respect, the simulation tools make no exception when the ISI of the floor is of interest. In other words, the whole chain must be modelled correctly to achieve results corresponding the real equivalent. When focusing on the excitation, the force driving the structure must be known.

Requirements for the most widely used standardized impact sound source, the ISO standard tapping machine (STM), have been presented in the standards ISO 10140–5 [6] and ISO 16283–2 [7]. The STM has five steel hammers (mass of 500 g) which have spherical impact surfaces with curvature radius of 500 mm. The hammers are repeatedly dropped from 40 mm height one at the time on to the floor two times per second. This results in a total repetition rate of 10 Hz and the rate is 2 Hz for a single hammer. An essential feature of the STM is that the produced impact force depends on the interaction between the hammers and the floor [8,9]. The force spectrum produced by the apparatus, in terms of the magnitude spectrum, is constant on bare concrete slabs whereas on wooden floors the spectrum depends on the floor configuration [10]. The theoretic range of level difference of the spectrum is 6 dB in the low-frequency range, and the difference rapidly expands with the increasing frequency [8].

Several analytical models describing the impact force excitation generated by the STM have been presented in the literature. The models could roughly be divided into two categories based on their applicability for different types of structures: the simple models for stiff and heavy floor systems, such as concrete floors, and the general models applicable also for elastic floors. The simple models were presented by Heckl and Rathe [11], Lindblad [12], Vér [13], Cremer et al. [14], and Scholl and Maysenhölder [15]. Later on, the models of Lindblad [12], and Vér [13] have been further developed by Brunskog and Hammer [8], and Griffin [16], respectively. The general models were derived by Brunskog and Hammer [8], Rabold et al. [17], Wittstock [18] and Amiryarahmadi et al. [19]. Coguenanff et al. [20] presented a probabilistic model of the impact force generated by the STM. Thorough comparisons between some of the models can be found for example in refs. [8,17].

* Corresponding author.
E-mail address: jesse.lietzen@tuni.fi (J. Lietzén).

https://doi.org/10.1016/j.engstruct.2022.114855
Received 11 April 2022; Received in revised form 20 July 2022; Accepted 17 August 2022
Available online 2 September 2022

The simple models [11–14,16] assume a hard slab surface and a large driving-point impedance of the slab compared to the mass impedance of the hammer. Thus, these models are mainly suitable in describing the interaction between the STM and concrete floors. Even though the model of Scholl and Maysenhölder [15] represents the effect of the floor on the interaction by the mass of the floor, the model does not fully describe the interaction between the STM and wooden slabs [8]. In addition to bare concrete slabs, the models [12,13,15,16] can consider the effect of resilient floor coverings on the impact force on concrete slabs. In [8] these properties of the model of Lindblad [12] were applied by using the stiffness in the model to describe the local deformation of the slab and the resistance part to represent the energy transportation within the slab. In this manner, the model [8,12] has been used, e.g., by Mosharrof et al. [21] for wooden slabs.

The general models [8,17,18] can consider complex features of the floors making them better suitable for describing the interaction between the STM and the wooden floors. The model by Brunskog and Hammer [8] has been defined in frequency domain and it divides the frequency-dependent mobility of the slab into local and global parts. This division has also been used by Rabold et al. [17] where they presented models both in time and frequency domains taking into account a transient process of the relative velocities between the hammer and the slab. Thus, their models [17] suggest that the force excitation changes in time until reaching the steady state. The model of Wittstock [18] describes the contact between the hammer and the floor with a frequency-independent stiffness and a loss factor, and the global effects by driving-point mobility of the plate. The models [8,17] were developed for the needs of the ISI calculation of wooden floors, whereas Wittstock [18] was characterising the interaction between the hammers of the STM and an infinite reception plate, thus making his model better suitable for this special case.

The models [8,17], however, have few shortcomings regarding their use in the ISI simulations of the wooden floors. First, the models [8,17] require detailed information from the floor, such as the local and global driving-point mobilities, as input data to determine the impact force driving the floors. In a general situation of a complex wooden floor this means that, e.g., finite element models of the floor are required to model the sole excitation. Secondly, considering the temporally variable excitation process, as in [17], makes the calculation of the impact force tedious in comparison with the other models. According to a recent study [10], considering this kind of behaviour is not needed to describe the impact force excitation on wooden floors. Thirdly, the models [8,17] do not consider the geometric non-linearity caused by the spherical impact surfaces of the hammers. This effect is taken into account by Amiryarahmadi et al. [19] who modelled the contact force in time domain by applying non-linear Hertzian contact theory. However, using Boussinesq expression to describe the stiffness due to the local deformation [19] does not fully correspond to the behaviour of a wooden slab near the point of excitation [8].

An interesting and elaborate technique to compute the impact force excitation would be to simulate the impact itself by using a FEM tool. First benefit from this is that the method can be implemented as a part of the simulation process. Secondly, modern FEM tools allow to consider the non-linear behaviour of the contact between the hammers and the floor. Third, the floor could be modelled using complex material models and geometries with very few practical restrictions. In this study, we apply the techniques used in the field of *computational impact mechanics* to simulate the impact force generated by the STM. The field uses explicit time integration and FEM (later briefly called *explicit dynamics analysis*) for impact studies [22,23]. The use of explicit dynamics analysis can be justified with its applicability to compute short and complex non-linear impacts.

The object of this study is to present a procedure to determine the impact force excitation generated by the STM on a wooden floor by explicit dynamics analysis. With a post-processing procedure, the results from the analysis can be used to determine the point forces driving the simulation models in time and frequency domains. To demonstrate the use of the explicit dynamics analysis, simulations have been performed for a wooden cross-laminated timber (CLT) slab by imitating an experimental measurement situation. The second purpose of this study was to investigate how to model a CLT slab in sufficient detail and which parameters are most important to the results. This is an essential matter from acoustical engineers' and researchers' point of view when they are dealing with developing mathematical models predicting the ISI of wooden floors. The latter has been investigated by means of a sensitivity analysis.

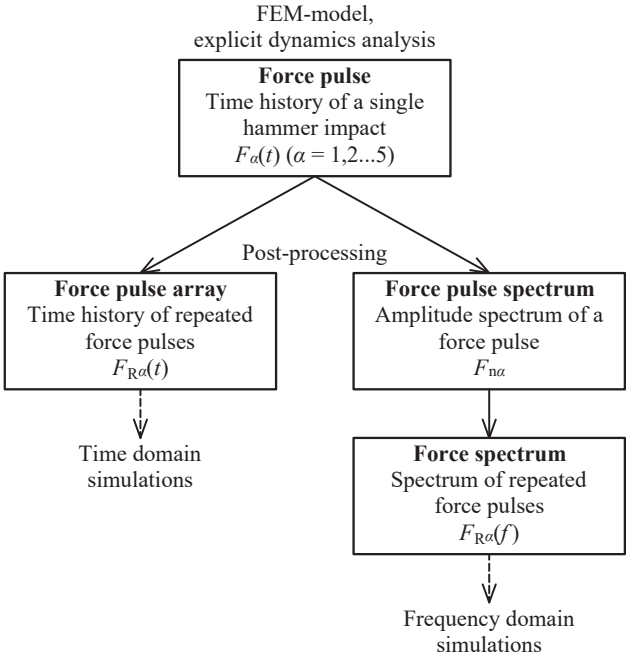

Fig. 1. Flowchart of the procedure for determining the point force generated by the STM.

2. Materials and methods

2.1. Procedure for determining the force generated by the STM

Impact force excitation generated by the STM on floors can be determined by a two-stage procedure illustrated in Fig. 1. The procedure aims to define the point force driving the floor both in time and frequency domains. These again can be utilized in ISI prediction models. First, the force pulse exerted by each of the five hammers must be known. At this stage, explicit dynamics analysis (FEM) is applied since it cost-efficiently enables describing the non-linear behaviour of the impact between the hammer and the floor. The second stage involves post-processing separately for time and frequency domain simulations. In the post-processing, the force pulses are converted into force quantities describing continuous operation of the STM.

Force pulse simulations are carried out within the time of contact, and when the hammer and the floor are disconnected no force driving the floor occurs. Thus, time history of the force $F_\alpha(t)$ of a single hammer α can be formulated extending the pulse signal with zeroes until the end of the period $T_r = 0.5$ s. In time domain, the excitation describing the continuous behaviour of the STM is a time history of repeated force pulses [8]. In frequency domain, the continuity is described with a Fourier spectrum for the repeated force pulses [8,18]. The force pulse array $F_{R\alpha}(t)$ and the force spectrum $F_{R\alpha}(f)$ can be determined for hammer α (α = 1,2…5) as follows:

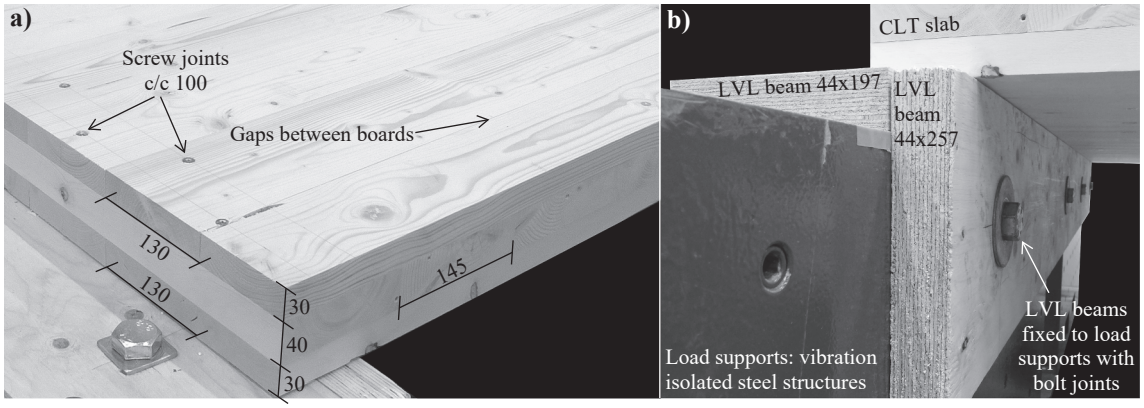

Fig. 2. CLT slab from a corner view (a) and supporting structures below another supported edge of the slab (b). Dimensions are presented in millimetres.

$$F_{\mathrm{R}\alpha}(t) = \sum_{n=-\infty}^{\infty} F_{\alpha}(t - nT_{\mathrm{r}}(1+k)) \tag{1}$$

$$F_{\mathrm{R}\alpha}(f) = \sum_{n=-\infty}^{\infty} F_{n\alpha}\delta(f - nf_{\mathrm{r}}) \tag{2}$$

where the constant k depends on the order of the hammer fall, $F_{n\alpha}$ is the amplitude of discrete frequency components, $f_r = 1/T_{\mathrm{r}}$ is the repetition rate for a single hammer, $\delta(\bullet)$ denotes the Dirac delta function, and $i = \sqrt{-1}$ represents the imaginary unit [8,18]. When the impact order of the hammers is 1 – 3 – 5 – 2 – 4, k gets values:

$$k = \begin{cases} 0, if\, \alpha = 1 \\ 1/5, if\, \alpha = 3 \\ 2/5, if\, \alpha = 5 \\ 3/5, if\, \alpha = 2 \\ 4/5, if\, \alpha = 4 \end{cases} \tag{3}$$

The amplitude spectrum for a force pulse can be determined with a Fourier transform:

$$F_{n\alpha} = \frac{1}{T_r}\int_0^{T_r} F_{\alpha}(t - nT_{\mathrm{r}}(1+k))e^{-2\pi \mathrm{n}i/T_r}dt \tag{4}$$

which represents a two-sided presentation of the amplitude spectrum of the force $F_{\alpha}(t)$ [8]. The shift of the pulse signal leads to a phase shift of the force for all but the first impacting hammer [18]. For simulation purposes, we are interested of the single-sided amplitude spectrum of the force. This can be achieved by taking the positive side of the complex two-sided spectrum and multiplying it by a value of two.

As seen from **Eqs. (1–2)**, the only unknown is the time history of the force $F_{\alpha}(t)$ of a single hammer. A simulation procedure to determine the force pulse has been shown in Section 2.3. The simulations imitate the experiments presented in Section 2.2.

2.2. Experiments

The impact force excitation generated by the STM was investigated by experiments with an instrumented STM on a CLT slab [10]. The centre hammer of the apparatus was modified and equipped with a force sensor which was used to determine the impact force input into the floor. The force sensor lied between the hammer body and the modified hammer head. The hammer together with the equipment fulfilled the requirements for the tapping machines presented in the standards [6,7]. Since the force driving the floor $F_{\mathrm{floor}}(t)$ was of interest but the force was measured between the hammer body and the hammer head, the sensor force signal $F_{\mathrm{sensor}}(t)$ was corrected based on the mass difference of the total hammer and its body:

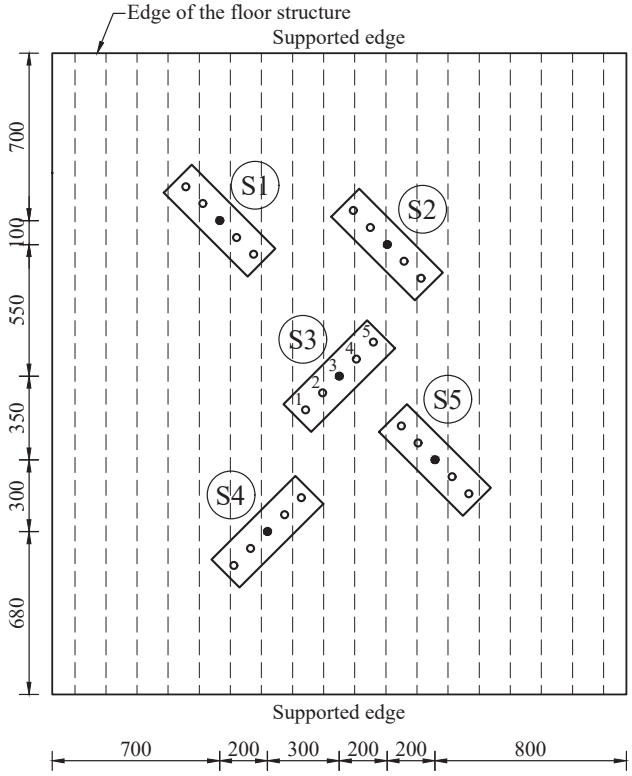

Fig. 3. Source positions S1–S5 on the floor structure (black circles). The rectangular boxes and the circles illustrate the orientation of the ISO tapping machine and the other hammers, and the dotted lines the board edges of the outer lamellae. Hammers for the tapping machine at source position S3 are numbered. Dimensions are presented in millimetres.

$$F_{\mathrm{floor}}(t) = \frac{m_h}{m_h - m_c}F_{\mathrm{sensor}}(t) = 1.061 \cdot F_{\mathrm{sensor}}(t) \tag{5}$$

where m_h is the total mass of the instrumented hammer (503 g), and m_c denotes the mass of the hammer head (29 g). For more information from the hammer instrumentation and the experiments, see [10].

2.2.1. Floor slab

The floor slab under study was a 100 mm thick 3-layered CLT slab which had lamellae of thicknesses 30, 40, and 30 mm as depicted in Fig. 2**a**. Individual boards of the slab were attached to each other only from their broader sides, i.e., the narrow sides of the boards were unglued. Therefore, slight gaps between the boards were present and their

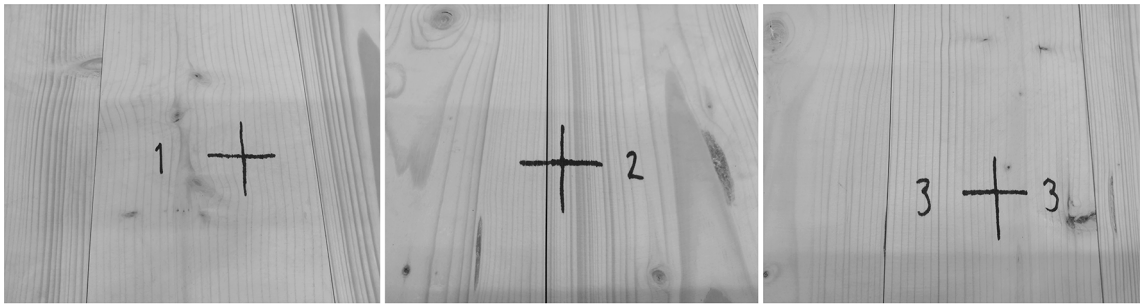

Fig. 4. Locations of the source positions S1, S2, and S3 and their distances from the board edges.

Table 1
Distances of the source positions S1–S5 from the board edges. The values follow the slab orientation depicted in Fig. 3.

Source position	Distance from the board edges [mm]	
	Left	Right
S1	85	45
S2	5	125
S3	65	65
S4	25	105
S5	75	55

maximum width was 1 mm [24]. Main widths of the boards in the outer lamellae and in the centre of the slab were 130, and 145 mm, respectively. Fig. 2**a** illustrates the CLT slab from its corner, where most of the abovementioned features can be seen.

Span of the CLT slab was 2.68 m and the outer layers of the slab ran parallel to this bearing direction. The width of the slab was 2.4 m. The slab was supported from its both ends to stiff laminated-veneer-lumber (LVL) beams with screw joints (Fig. 2**a**). The long sides of the slab were unsupported. The LVL beams were fixed into vibration isolated steel structures placed on the floor of the laboratory (Fig. 2**b**). This was done to prevent the possible vibrational background noise caused in the surroundings of the experiments. For more information on the structures and their installations, see [10]. As illustrated by Fig. 2, major part of the slab was constructed from timber sawn near the pith of the tree. Thus, the lamellae mainly consisted of heartwood where annual rings of the trees were visible.

2.2.2. Measurement positions

The force measurements were carried out at five source positions S1–S5 on the floor (Fig. 3). At each source position, the STM was oriented at a 45° angle to the bearing direction of the CLT slab. The position S3 was located at the centre of the floor structure. During the measurements, the STM operated normally on the floor and the time history of the impact force subjected to the sensor was recorded. The measurement duration at each position was approximately 30 s and the sampling frequency was 12800 Hz. Because the tapping machine drops its hammers two times per second, the number of full impacts generated by the hammer at the source positions was 60 or 61.

Fig. 4 shows an example of the location of the source positions S1, S2, and S3 and their distances from the closest board edges. The position S3 lied in the centre of the board and the S2 was in the furthermost location from the centre; the other positions lied between these extremes. The distances from all the source positions to the closest board edges have been shown correspondingly in Table 1.

2.3. Simulations

The force pulse generated by a hammer of the STM was simulated applying explicit dynamics analysis. Simulations were performed using a FEM program Ansys LS-DYNA (smp s R10.1.0 Revision: 123264).

2.3.1. Governing equations

Collision of two bodies (a hammer and a slab) can be described by a mathematical model in which the time-dependent motion of two structural domains Ω_{hammer} and Ω_{slab} causes contact between them. The domains are separate and their respective boundaries $\partial\Omega_{hammer}$ and $\partial\Omega_{slab}$ do not intersect during the collision since the deformed bodies cannot penetrate. Thus, their equations of motions remain uncoupled [25].

For brevity, the system and its finite element formulation is shown for a general domain Ω enclosed by its boundary $\partial\Omega$. The partial differential equation of motion describing the system inside the domain Ω is:

$$\nabla\cdot\boldsymbol{\sigma}+\rho\boldsymbol{f}=\rho\ddot{\boldsymbol{x}} \tag{6}$$

where $\boldsymbol{\sigma}$ is the Cauchy stress tensor, ρ is the density, $\boldsymbol{f}$ is the body force density, and $\ddot{\boldsymbol{x}}$ is the acceleration (second-order time derivative of displacement) [23,25]. The equation must satisfy the boundary conditions for traction, displacement, and contact discontinuity on boundaries $\partial\Omega_1$, $\partial\Omega_2$, and $\partial\Omega_3$, respectively. These boundary conditions are:

$$\boldsymbol{\sigma}\cdot\boldsymbol{n}=\boldsymbol{t}(t) \tag{7}$$

$$\boldsymbol{x}(X_\alpha,t)=\boldsymbol{D}(t) \tag{8}$$

$$(\boldsymbol{\sigma}^{+}-\boldsymbol{\sigma}^{-})\cdot\boldsymbol{n}=0 \tag{9}$$

where $\boldsymbol{n}$ represents a unit outward normal to a boundary on $\partial\Omega$, $\boldsymbol{t}$ is the applied traction load, $\boldsymbol{D}$ is the specified displacement [23,25].

The deformation is expressed in terms of the convected coordinates [25]:

$$x_i=x_i(X_\alpha,t) \tag{10}$$

where $X_\alpha(\alpha=1,2,3)$ represents a point in undeformed geometry and $x_i(i=1,2,3)$ a moved point in the same fixed rectangular cartesian coordinate system. At time $t_0=0$, the given initial displacement $\boldsymbol{X}^0$ and velocity $\boldsymbol{V}^0$ inside the domain Ω are, respectively [25]:

$$x_i(\boldsymbol{X},0)=X_i^0 \tag{11}$$

$$\dot{x}_i(\boldsymbol{X},0)=V_i^0(\boldsymbol{X}) \tag{12}$$

After a few mathematical operations, the weak integral form of the equilibrium equation becomes:

$$\int_\Omega\rho\ddot{\boldsymbol{x}}\delta\boldsymbol{x}d\Omega=-\int_\Omega\boldsymbol{\sigma}\delta\boldsymbol{x}d\Omega+\int_\Omega\rho\boldsymbol{f}\delta\boldsymbol{x}d\Omega+\int_{\partial\Omega_1}\boldsymbol{t}\delta\boldsymbol{x}ds \tag{13}$$

where $\delta\boldsymbol{x}$ denotes the variation of displacement, c.f. principle of virtual work [25]. By applying an approximation for the displacement field, we superimpose a mesh of finite elements [25]:

$$x_i(X_\alpha,t)=x_i(X_\alpha(\xi,\eta,\zeta),t)=\sum_{j=1}^{k}N_j(\xi,\eta,\zeta)x_i^j(t) \tag{14}$$

where N_j are shape functions describing the displacement field within the elements. The finite element formulation of the problem is:

$$\sum_{m=1}^{n}\int_{\Omega}\rho \boldsymbol{N}_m^T\boldsymbol{N}_m\boldsymbol{a}d\Omega=\sum_{m=1}^{n}\left(-\int_{\Omega}\boldsymbol{B}_m^T\boldsymbol{\sigma}d\Omega+\int_{\Omega}\rho\boldsymbol{N}_m^T\boldsymbol{b}d\Omega+\int_{\partial\Omega_1}\boldsymbol{N}_m^T\boldsymbol{t}ds\right) \tag{15}$$

where $\boldsymbol{a}$ is the nodal acceleration vector, $\mathbf{B}$ is the strain–displacement matrix, and $\boldsymbol{b}$ is the body force load vector [25]. This equation can be recognized as one form of Newton's second law in matrix presentation [23,25]:

$$\mathbf{M}\boldsymbol{a}^n=\mathbf{F}^n \tag{16}$$

The dynamics of the system, i.e., the nodal acceleration, velocity and displacement vectors $\boldsymbol{a}$, $\boldsymbol{v}$, $\boldsymbol{u}$ in time domain, respectively, is solved by applying explicit time integration. The commonly used central difference time integration method is also implemented in LS-DYNA [25]. The method allows direct calculation of the nodal acceleration vector:

$$\boldsymbol{a}^n=\mathbf{M}^{-1}\mathbf{F}^n \tag{17}$$

$$\boldsymbol{v}^{n+1/2}=\boldsymbol{v}^{n-1/2}+\boldsymbol{a}^n\Delta t^n \tag{18}$$

$$\boldsymbol{u}^{n+1}=\boldsymbol{u}^n+\boldsymbol{v}^{n+1/2}\Delta t^{n+1/2} \tag{19}$$

where.

$$\Delta t^{n+1/2}=(\Delta t^n+\Delta t^{n+1})/2 \tag{20}$$

Because the mass matrix $\mathbf{M}$ is diagonal, instead of inverting the mass matrix, the nodal acceleration $\boldsymbol{a}$ in each time step is calculated by a simple division. After solving the nodal displacement vector $\boldsymbol{u}$, the initial geometry is updated, and the force matrix $\mathbf{F}$ is recalculated. This loop is repeated until the time of interest is reached. [23,25].

As seen from the above, the diagonal mass matrix $\mathbf{M}$ increases the efficiency of the time integration. This is one of the main features of the explicit dynamic method and means that the system consists of lumped elements, which are calculated separately. The diagonal mass matrix can be used since there is no loss of accuracy in comparison with the use of the consistent mass matrix [23,26]. Moreover, this leads to a requirement that the sound wave cannot travel to the other side of the element within the time step Δt. Therefore, to ensure a stable solution, the time step must be set below the critical time step:

$$\Delta t_{crit}=2/\omega_{max} \tag{21}$$

where ω_{max} denotes the largest elemental natural frequency of the structure in consideration. However, to increase the accuracy of the model, it is beneficial to use smaller time steps (or reduce the element sizes) [23].

The contact between the two domains Ω_{hammer} and Ω_{slab} is primarily modelled as frictional using a Coulomb formulation [25]. Thus, the frictional force at time n ($\boldsymbol{f}_n$) can be calculated, when the frictional coefficient μ, and the tangential contact force F_y are known:

$$F_y=\mu|\boldsymbol{f}_n| \tag{22}$$

where

$$\mu=\mu_d+(\mu_s-\mu_d)e^{-c|\boldsymbol{v}|} \tag{23}$$

where μ_s denotes the static and μ_d the dynamic frictional coefficients, and $\boldsymbol{v}$ is the relative velocity between the element nodes in contact.

2.3.2. Model settings and geometry

For the contact problem between the hammer and the CLT slab, imitating the experiments (see Section 2.2), the terms including the effects of both the body force loads $\boldsymbol{b}$ and the tractions on the boundary $\boldsymbol{t}$ in Eq. (11) were regarded insignificant. Thus, the gravitational forces and the load from the legs of the STM to the slab were neglected in the simulations. The vertical displacements on the supported edges (see Fig. 3) were set to 0 mm. The FEM-model was built by using linear 8-node hexahedron solid elements of type −2 (LS-DYNA) with modified Jacobian matrix to prevent locking of elements during the impact [25].

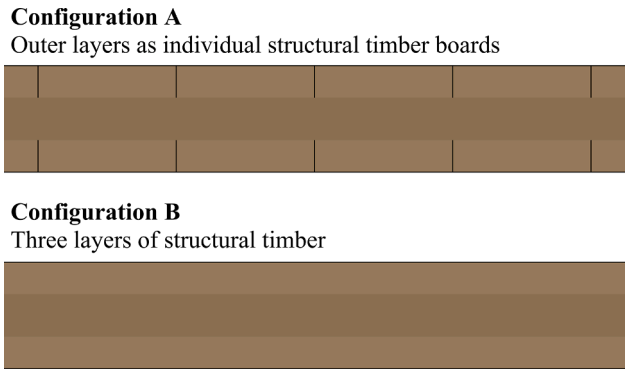

Fig. 5. Slab modelling configurations. Configuration A has primarily been applied in the simulations.

In the experiments [10], it was found out that there was little temporal variation in the measured impact force pulses. It was concluded that the vibration of the slab did not significantly contribute to the force pulses [10]. Because of this, initially the CLT slab was at rest in the simulations. The hammer of the STM was dropped from a height of 40 mm to the CLT slab. Hence, the initial velocity of the hammer $\boldsymbol{V}^0$ was 0.886 m/s and the $\boldsymbol{X}^0$ of the CLT slab was zero (c.f. **Eqs. (11–12)**). The simulations for the model validation were carried out at each source position S1–S5 (Fig. 3).

The contacts between the hammer and the slab were modelled by using a penalty method (LS-DYNA keyword: *CONTACT_AUTOMATIC_SINGLE_SURFACE [27]) and the contact forces were read with a force transducer contact (*CONTACT_FORCE_TRANSDUCER_PENALTY [27]). Both the static and the dynamic frictional coefficients μ_s and μ_d were set to a value 0.5. Hence, according to **Eq. (23)** the frictional coefficient μ reduces to $\mu=\mu_d=0.5$. The hammer of the STM represented a simplified model of the instrumented hammer used in the experiments (see Section 2.2). The impacting head of the hammer was modelled to represent closely the real hammer head in the measurements, but the body with the sensors and additional parts of the hammer was modelled as a simplified cylinder with diameter of 20 mm. The height of the cylinder was adjusted so that the total mass of the modelled hammer corresponded to $m_h=503$ g [10]. In the analyses the hammer was treated as an ideal impact source and, thus, all the possible imperfections of the STM [6,18], such as the possible variation in velocity at impact, were neglected.

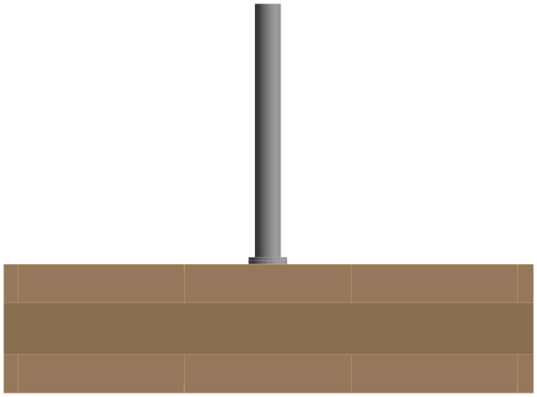

Fig. 6. Geometry of the model near the impact area.

Table 2
Material parameters describing the linear isotropic elastic behaviour of the hammer. The bolded values are the average parameters presented by the standards EN 1993–1-1 and EN 1993–1-4 [29,30].

Material parameter	ρ [kg/m^3]	E [MPa]	ν [-]
Steel hammer	7 641	**205 000**	**0.3**

The simulations were carried out for two slab modelling configurations (Fig. 5) where the structural timber layers were meshed together. Thus, it has been assumed that glue layers between structural timber layers are very thin and the glue perfectly connects the timber layers. In the configuration A, the outer lamellae of the CLT slab were modelled as individual structural timber boards. In this configuration, no contacts were defined between the narrow sides of the lamellae. Note, however, that this procedure prevents the boards from contacting adjacent boards. In the configuration B, the CLT slab was modelled with three continuous structural timber layers. In both configurations the direction of the boards determined the principal axes of the lamellae. Since the configuration A presents the slab in the experiments in a more detailed way, this configuration has primarily been applied in the simulations. The slab configuration B was used in the sensitivity analysis.

Fig. 6 shows the geometry of the model near the impact area when the hammer was at the source position S3 in the centre of the CLT slab's surface. In the beginning of the simulation, the tip of the hammer head was in contact with the slab in a single point and the hammer was just dropped to the slab.

2.3.3. Material parameters

The hammer of the STM was modelled as linear isotropic elastic material (*MAT_ELASTIC [28]), and the boards of the slab as linear orthotropic elastic material (*MAT_ORTHOTROPIC_ELASTIC [28]). Table 2 shows the material parameters used to describe the behaviour of the steel hammer. Density of the hammer head was determined based on its mass (29 g) and known volume. The density of the whole hammer was assumed to be the same. Modulus of elasticity E, and the Poisson's ratio ν of the hammer were not known but they were presumed to correspond with the average parameters of structural and stainless steels [29,30].

According to the European Technical Assessment for the CLT slab [24], the wood species used in the product was European spruce or equivalent softwood. In this study, it has been presumed that the wood species used in the lamellae was European (or Norway) spruce (*Picea abies* (L.) Karst.) and no other wood species was present to a significant extent. The individual boards of the CLT slab may be described as a linear orthotropic elastic material whose three principal axes are longitudinal (L), radial (R), and tangential (T) axes with respect to the fibre direction and annual rings of the timber [31]. In major part of the simulations, these axes were assumed to correspond the local coordinate axes of the CLT lamellae in a cartesian coordinate system. However, in a part of the sensitivity analysis, the material parameters were partly in a cylindrical coordinate system by locally rotating the system. Strength class of the boards according to standard EN 338 [32] was mainly C24 but 10 % of the material could be included from the class C16 [24]. In addition to the density ρ of the material, the standard EN 338 presents three of the nine independent constants describing the orthotropic behaviour of the boards: moduli of elasticity E_L and E_T, and shear modulus G_{LT}. These parameters present mean characteristic values for structural timber made from softwood in corresponding strength classes [32].

Values for all the parameters needed to completely describe the linear orthotropic elastic material have not been presented by the standard EN 338. The remaining six constants E_R, G_{LR}, G_{RT} and the Poisson's ratios ν_{LR}, ν_{LT}, and ν_{TR} have been derived from the measurement results for the Norway spruce presented by Keunecke et al. [33]. This has been carried out by scaling the results presented by the study [33] for the modulus of elasticity E_R and the shear moduli G_{LR}, and G_{RT} with respect to the values of E_L and G_{LT} presented by the standard EN 338, respectively. The Poisson's ratios have been adopted straight from [33] by presuming their dependence on the strength classes insignificant. This approach was used to determine the material parameters for the European (or Norway) spruce in strength classes C24, C16, and C30 (Table 3). The values for C24 have primarily been used to describe the behaviour of the individual boards of the CLT slab under study. The values for C16, and C30 have been used in the sensitivity analysis.

2.4. Calculation results for the force pulses

The contact force pulse $F(t)$ during the impact was derived from the simulations by filtering the result with a Butterworth filter of which cut-off frequency was 6000 Hz (in building acoustics, the most interesting frequency range is 20–5000 Hz). In addition to the time history, a two-sided amplitude spectrum of the force F_n (**Eq. (4)**), a mechanical impulse I, i.e., change in the momentum, and a low-frequency force F_{lf} were calculated. The relation between the mechanical impulse I, and low-frequency force F_{lf} is:

$$F_{lf} = \frac{1}{T_r} I = \frac{1}{T_r} \int_0^{T_r} F(t) dt \tag{24}$$

when the low-frequency force corresponds to the limit value of F_n, when frequency f approaches 0 Hz [8]. To achieve comparable scalars describing the magnitude and the duration of the force pulse $F(t)$, the peak value of the force (F_{peak}) and the length of the pulse (T_{pulse}) were also determined.

2.5. Model validation and sensitivity analysis

The finite element model was validated by comparing the simulation results with the measurement results from the experiments (see Section 2.2). In the model, the strength class of the CLT slab was C24 (see Section 2.3.3), and the simulations were done applying the slab modelling configuration A (Fig. 5). The modelling process was carried out in two steps: first, the element mesh was determined based on a mesh convergence study; secondly, the chosen mesh was used in the calculations. The simulation results were received from the body interaction contact between the hammer and the slab imitating the experimental situation [10]. The validated model was further applied for sensitivity analysis. Purpose of this analysis was to investigate which parameters are the most important or sensitive to the results and how to model a CLT slab in sufficient detail. Moreover, the validated model was applied to compute force results for all hammers in an example situation. These results were post-processed to reach input values applicable for time and frequency domain simulations as illustrated in Section 2.1.

Table 3
Material parameters describing the linear orthotropic elastic behaviour of European (or Norway) spruce in strength classes C24, C16, and C30. The bolded values are the parameters presented by the standard EN 338 [32]. The remaining values have been derived from the measurement results presented by Keunecke et al. [33].

Strength class	ρ [kg/m^3]	E_L [MPa]	E_R [MPa]	E_T [MPa]	ν_{LR} [-]	ν_{LT} [-]	ν_{TR} [-]	G_{LR} [MPa]	G_{LT} [MPa]	G_{RT} [MPa]
C24	**420**	**11 000**	537	**370**	0.36	0.45	0.21	725	**690**	62
C16	**370**	**8 000**	391	**270**	0.36	0.45	0.21	526	**500**	45
C30	**460**	**12 000**	586	**400**	0.36	0.45	0.21	788	**750**	68

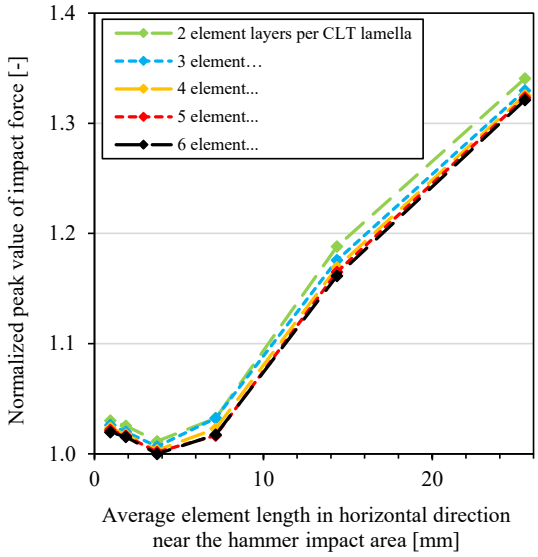

Fig. 7. Mesh convergence study at source position S3.

3. Results

3.1. Validation results

As discussed in Section 2.3.1, it is important to have a valid mesh to get relevant results from the explicit dynamics analysis. Thus, the model validation began with a mesh convergence study carried out at the source position S3. In the study, the element mesh of the CLT slab was varied in two different ways. First, the number of element layers through one CLT lamella ranged between two and six. Secondly, the average element length in horizontal direction near the impact area was reduced in steps from 25 mm to 1 mm. Outside the impact area, the element length in the horizontal direction was set to approx. 28 mm. The mesh of the hammer was kept constant in the convergence study with element lengths between 1.4 and 3.0 mm and 2.4 to 8.6 mm for the hammer head and body, respectively.

Fig. 7 shows the results of the mesh convergence study by normalizing the determined peak values of impact force with the lowest result of the study. The figure illustrates how the element mesh affects the results: when the mesh is coarse, the CLT slab is overly stiff and leads to overestimated impact force; when the element length is decreased, there exists an element dimension after which a denser mesh does not

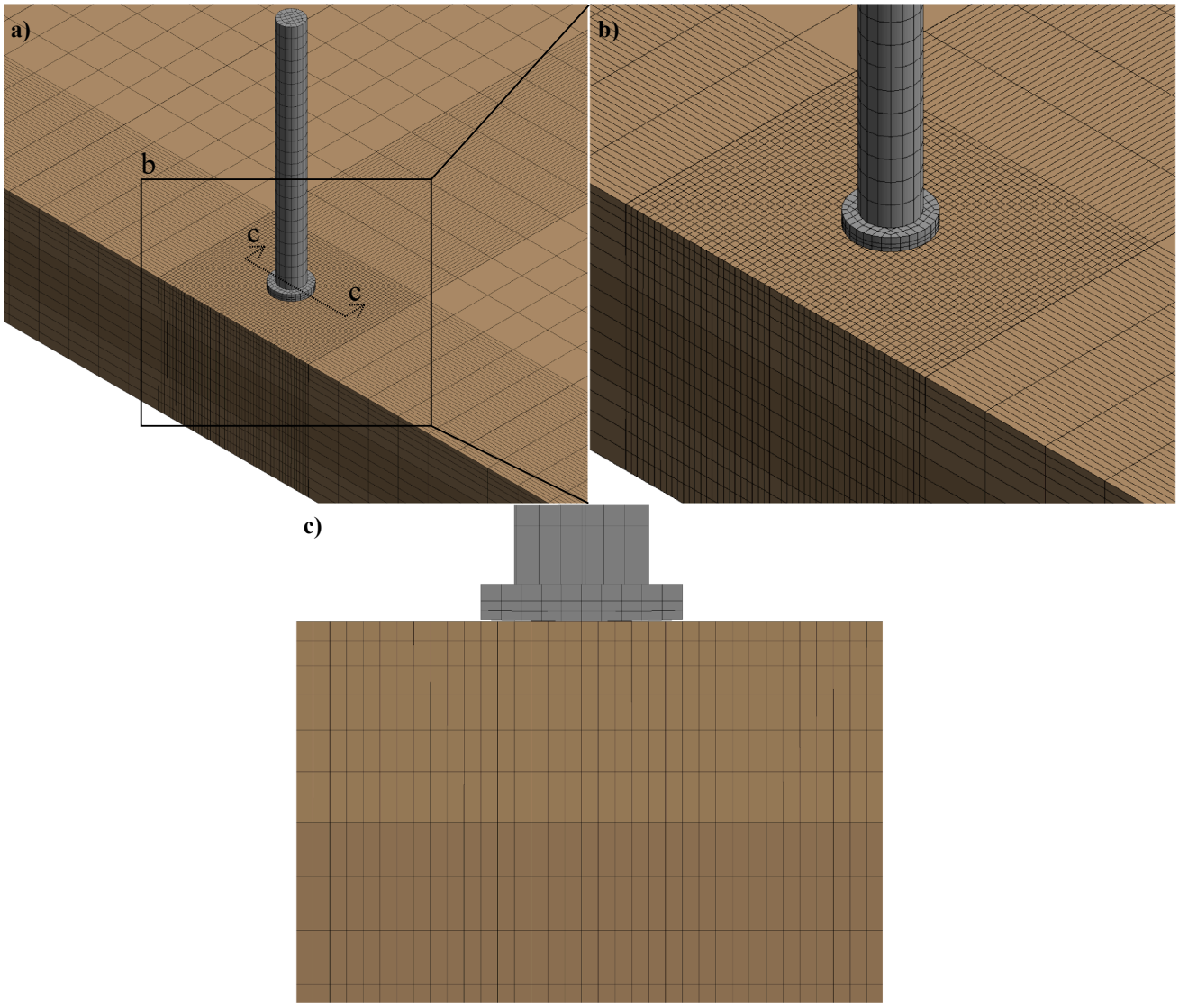

Fig. 8. Element mesh of the hammer and the slab: a) hammer and impact area, b) impact area magnified, c) cross section of impact area. Note that the elements on the left side of the Fig. 8a and 8b have been hidden to highlight the mesh in the sectional direction.

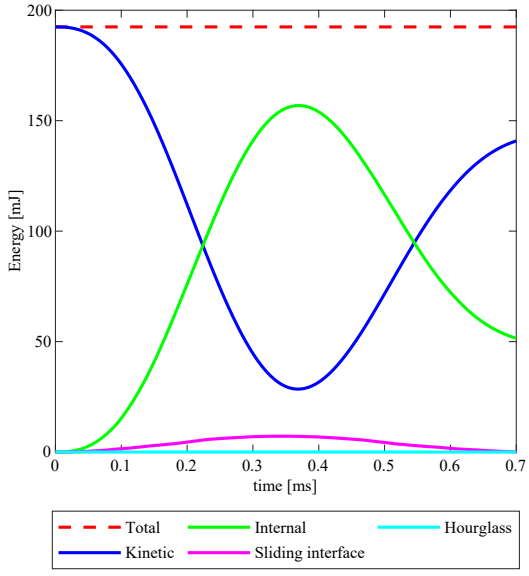

Fig. 9. Energy balance of the simulation.

drastically improve the accuracy of the model. Furthermore, the figure shows that the convergence decelerates with shorter horizontal element lengths. This is probably influenced by the size and aspect ratios of the elements of the hammer and the CLT slab further away from the impact area.

Based on the results of the mesh convergence study (Fig. 7), the mesh used in the analysis was constructed from elements of average length 2.5 mm near the impact area. Elsewhere the mesh was coarser, and the element length was set to approx. 28 mm. Furthermore, the upper CLT lamella was formed from six, the centre lamella from five, and the lowest lamella from four elements through the thickness of the layer. This criterium was kept for the whole slab as in the mesh convergence study. For the whole model at the source position S3, the number of elements was 267,724 and the number of nodes 313244. Fig. 8 illustrates the element mesh near the impact area including the hammer and the slab.

Due to the collision of the hammer and the CLT slab, kinetic energy transfers into the slab, and the energy balance is a function of time. An example of this has been shown in Fig. 9 by using the model described above (source position S3). The total energy of the system was 192.5 mJ, which initially consisted of kinetic energy only. Since energy cannot transfer outside the modelled system, the total energy stays at this constant level. During the interaction of the hammer and the slab kinetic energy transfers into internal energy and into the energy of the sliding interface. The change in the kinetic energy before and after the collision represents energy dissipation. Hourglass energy during the impact is zero because of the chosen element type (see Section 2.3.2). Nonzero hourglass energy would imply nonphysical behaviour of the model.

Fig. 10 depicts the comparison of the simulated and measured force pulses in time and frequency domains. The figure shows the measured and the simulated contact force pulses $F(t)$ and magnitudes of their amplitude spectra F_n at the source positions S1…S5. To ease comparison, the measured force pulses have been centred according to the peak values of the simulation results. Hence the nonzero values before t_0. The peak value of the force F_{peak}, the low-frequency force F_{lf}, the mechanical impulse I, and the length of the pulse T_{pulse} have been presented in Table 4 for the measured and simulated force pulses. The measurement results presented in Fig. 10 and Table 4 have been reproduced from [10] by using a correction factor as in **Eq. (5)**.

Fig. 10 and Table 4 indicated reasonable equivalency of the measurement and simulation results. Thus, the simulation model was regarded valid. However, it is noticeable that the computational model led to minor spatial variation in comparison with the measurement results. The simulation seemed to closely predict the measured peak value of the force F_{peak} at the source positions S3, and S5. Additionally, the low-frequency force F_{lf}, and the mechanical impulse I of the simulation results were near equivalent with the measurement result at the source position S4. Minor discrepancies between the measurement and simulation results at the source positions S1, and S2 were prominent. Moreover, the lengths of the simulated force pulses were shorter than the measured values at all the source positions. This can be explained with the low time resolution of the measurements in comparison with the simulations [10]. The magnitude spectra of the simulation results resembled the measured spectra closely and minor differences were prominent at frequencies above 2000 Hz. In the low-frequency range, discrepancies between the measured and the simulated F_{lf} results correspond with a 0.7 dB level difference at the source position S2 [8]. At other positions differences were smaller.

The simulations produced results near the measured maximum both in time and frequency domains. As can be seen, there was little spatial variation in the simulation results whereas the measured results varied greater (Table 4). The source positions S3, and S5, where the maximum peak value of the force F_{peak} was measured, lied near the centre of the boards (Table 1). At these positions, the F_{peak} of the simulated force pulses also reached their maximum values. Moreover, the source position S2 lied at the furthermost location from the centre of the board. At this position, both the measured and simulated force pulses got their lowest values for F_{peak}. This behaviour suggests that the local properties of the CLT slab affect the impact force.

To study the importance of the local properties to the impact force pulse, deformation process of the slab under the hammer has been illustrated in Fig. 11. As an example, the figure depicts the total (elastic) deformation of the CLT slab during the impact from 0.1 to 0.7 ms at the source positions S1, S2, and S3. The results show that the maximum deformation occured straight under the tip of the hammer head and when the impact force pulse was near its peak value (cf. Fig. 10). Furthermore, only a minor part of the slab was deformed during the impact, which suggests that for a short impact the global behaviour of the slab is not of importance from the point of view of the single impact force pulse. Additionally, the non-linear interaction between the hammer and the slab can be seen from Fig. 11 since the contact surface between the hammer and the slab is a function of time. The effect of the local and global properties to the impact force and reasons causing the differences between the measurement results at different source positions were studied with the sensitivity analysis.

3.2. Sensitivity analysis

The sensitivity analysis was carried out in six phases. For the sake of simplicity, the sensitivity of different parameters on the simulation results have been shown by comparing the results for the peak values of the force F_{peak}. First, to study the effect of the global source position on the impact force, simulations with the validated model were repeated applying the slab configuration B (Fig. 5). The configuration ignores the gaps between the boards of the CLT slab but otherwise the computational model was created similarly than the model in validation. The simulations were carried out at all the source positions S1–S5, and the comparison of the F_{peak} with the measurement results and the results from the validated model have been shown in Fig. 12. According to the simulation results for the configuration B, the maximum change in the F_{peak} was 2.9 N between source positions S1 and S3, when the lowest levels occurred at S3. The results imply that the impact force pulse is insensitive to the global position of the hammer on the slab, but the local properties of the CLT must explain spatial variation in the measurement results. The sensitivity analysis was continued with the slab modelling configuration A and the analyses were performed at the centre of the CLT slab, c.f. the source position S3.

To further study the effect of the global properties on the impact force, the sensitivity analysis was continued in the second phase by

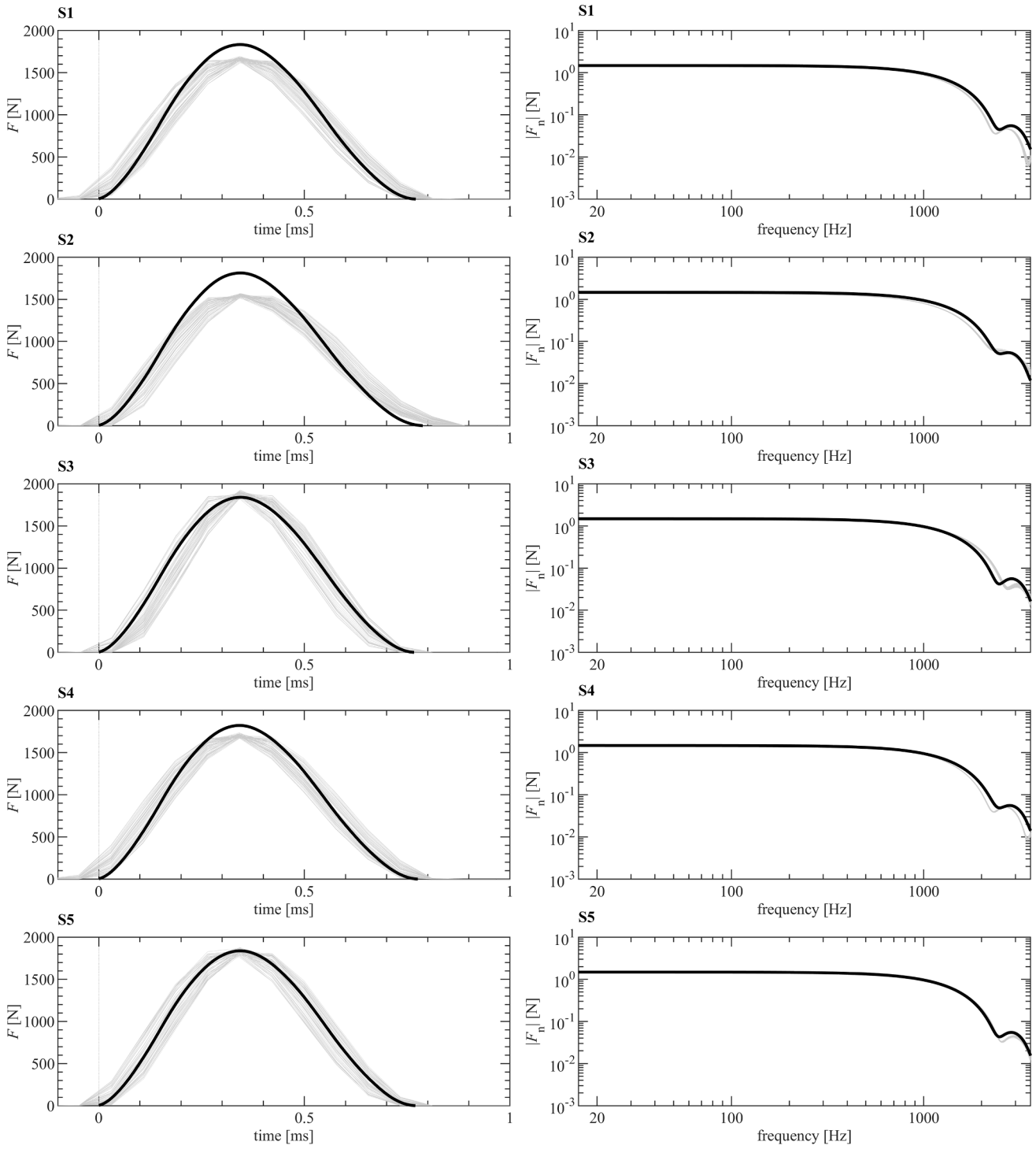

Fig. 10. Simulated contact force pulses $F(t)$ and magnitudes for their two-sided amplitude spectra F_n at the source positions S1…S5 (black lines) and the corresponding measurement results from the experiments [10] (thin grey lines). Note the overlapping of the results.

varying the CLT slab size (or the boundary conditions) by shortening the length and the width of the slab in 200 mm steps. The results of the study show that the floor size has minor effect on the peak value of the force and reducing the size of the floor does not significantly decrease the accuracy of the simulation results (Fig. 13). This occurred probably due to the short duration of the impact (less than 1 ms, see Table 4) when the reflecting stress wave did not reach from the boundaries of the CLT slab to the contact position within the time of impact even if the floor size was diminished. Thus, in the modelled situation it is justified to simulate the contact force pulse by reducing the size of the floor. The sensitivity analysis was proceeded with a CLT slab of size 1000 mm × 1000 mm to reduce calculation time.

Thirdly, the effect of the friction between the colliding bodies on the results was studied by changing the friction coefficients exaggeratedly from 0.5 to 0 and 1. The main motivation for the analysis was to find out if the friction coefficient is an important parameter for the analysis since exact values for different structures are not necessarily known. Fig. 14 shows the peak values of the force when the friction coefficients (both static and dynamic) between the hammer and the slab are 0, 0.5, and 1. The results indicate that the friction affects the results minorly. This

Table 4
Scalar values determined for the measured and simulated force pulses. Measured values show the average results based on all the measured force pulses at the corresponding source position.

Source position	Measured (M)/ Simulated (S)	F_{peak} [N]	F_{lf} [N]	I [Ns]	T_{pulse} [ms]
S1	M	1662.5	1.42	0.71	0.99
	S	1833.4	1.48	0.74	0.77
S2	M	1546.3	1.36	0.68	1.02
	S	1813.3	1.47	0.74	0.79
S3	M	1878.5	1.40	0.70	0.91
	S	1839.3	1.48	0.74	0.77
S4	M	1699.4	1.47	0.74	1.01
	S	1822.2	1.48	0.74	0.78
S5	M	1832.8	1.45	0.73	0.94
	S	1838.2	1.48	0.74	0.77

occurred probably due to the normal incidence of the hammer relative to the surface of the slab. The sensitivity analysis was continued with the friction coefficients 0.5.

The impact force is affected by local properties in the horizontal direction of the slab, as shown by Figs. 10–12. Because of this, the local effects in the sectional direction of the CLT slab were studied with two analyses. First, the effect of the strength class of the centre lamella on the results was analysed by varying it from C24 to C16 and C30 while the upper and the lower lamellae were C24. Secondly, the effect was analysed with introducing imaginary materials to the analysis by increasing the stiffness parameters of the lamellae so that the moduli of elasticity and the shear moduli were magnified tenfold (material X10). Physically this could represent material of a hard tree knot, but the intention was to consider the effect of a drastic change in stiffness of the material. The results of these analyses have been shown in Fig. 15. According to the results, the strength class of the centre lamella has a minor effect on the impact force, but drastic changes in the stiffness properties can have a major effect on the impact force especially if the upper lamellae changes (c.f. tree knots near the impact area).

The material parameters of real wood are not constant but vary depending on the tree and between the specimens [33]. Because of this, the effect of the material parameters of the boards on the impact force was studied. The motivation for the analysis was to find out if the differences of the material parameters would explain the discrepancies between the simulation and the measurement results and especially the variation between the measurement results between source positions. In the study, the calculations were conducted by varying a single material parameter at a time. The varied material parameters were the density ρ, moduli of elasticity E_L, E_R, and E_T, Poisson's ratios (ν_{LR}, ν_{LT}, and ν_{TR} simultaneously), and the shear moduli G_{LR}, G_{LT}, and G_{RT}. The range of the material parameters was such that the lower values correspond to the material parameters for spruce in the strength class C16 and the higher values to the parameters for spruce in the class C30 (see Table 3). The results for the analysis (Fig. 16) depict that the modulus of elasticity E_R, the shear modulus G_{LR}, and the density ρ have the greatest effect on the peak value of the force.

The CLT slab used in the measurements was mainly made from heartwood near the location of the pith (see Fig. 2). The boards were oriented so that the broad side closer to the pith could lay on either upwards or downwards in the slab. Thus, using the cartesian coordinate system describing the material of the timber boards is a simplification of the real situation. The effect of this simplification and the use of heartwood and sapwood on the results was analysed by replacing the cartesian coordinate system of the impacted upmost timber board with a locally rotated cartesian coordinate system with different origins from the pith. From the point of view of the boards, this corresponds to a cylindrical coordinate system. Boards from four different locations relative to the distance from the pith perpendicularly from the centre of the lower edge of the lamellae were studied: A) heartwood, distance from the pith 0 mm, B) heartwood of a large log, distance from the pith 100 mm, C) sapwood of a medium-sized log, distance from the pith 150 mm, D) sapwood of a large log, distance from the pith 500 mm (Fig. 17). In all the configurations, the radius from the origin pointed upwards in the normal direction of the board.

The analysis was carried out with a symmetrical half model with respect to the transverse direction of the top and bottom lamellae. The impact simulations were performed in 10 mm steps from the edge of the board (centre distance from the edge was 15 mm, cf. the radius of the hammer head) to the centre of the board. The results of the analysis have been depicted in Fig. 18 with different distances from the nearest board edges, the centre distance of the board being 65 mm. To ease comparison with the measurements and previously presented simulation results, the figure also shows the results for the source positions S1–S5 (see Fig. 12), and a polynomial trend line of order two for the measurement results (assumed symmetry of the results around the centre axis). The results clearly indicate that the differences in the measurement results can be explained with the presence of heartwood in the CLT slab. Hence, using rotated cartesian coordinate system improves the correlation between the measurement and the simulation results.

The sensitivity analysis confirms the insignificance of the global and importance of the local properties to the single impact force pulse. Additionally, the results of the analyses give reasons for the differences between the measurement results and the simulation results from the validated model.

3.3. Post-processed force results

To use the simulated force pulses as inputs for point forces in time or frequency domain ISI simulations, the results must be post-processed to describe the continuous operation of the STM. To demonstrate this procedure, the validated model was applied to compute the force pulse for each of the five hammers of the STM on the CLT slab at the source position S3. The simulated force pulses were post-processed according to Section 2.1. The post-processed force results have been depicted in Fig. 19 both for time and frequency domain simulations. The figure shows the force pulse array $F_{R\alpha}(t)$ for the two first pulses, and the single-sided force spectrum $F_{R\alpha}(f)$ for individual hammers at the source position. The time shift of the force pulses causes phase shift to the force spectra which can be seen as fluctuation of real and imaginary parts of the force spectra.

4. Discussion

4.1. Model applicability and findings

The model validation shows that the explicit dynamics analysis is applicable in predicting the impact force generated by the STM on a wooden slab (Fig. 10, and Table 4) when the calculation mesh is appropriate (Fig. 7) and the values for material parameters represent the behaviour of the slab. Comparison of the simulation and experimental results for the CLT slab indicated that in time domain, the measured force pulses vary more than the simulated ones with respect to the source position (Fig. 10). However, the finite element model seemed to closely predict the maximum force pulse regardless, which is a desirable effect considering ISI calculations (e.g., computing the normalized impact sound pressure level L_n) of wooden floors using the FEM. Discrepancies between the measurement results of different source positions can partly be explained with the different distances from the closest board edges. The differences between the simulated and measured values were, however, minor in the low-frequency range. Reasons explaining the differences between the measurement and simulation results, and the minor spatial variation of the simulation results (Fig. 10, and Table 4) were found in the sensitivity analysis. First, the material properties in the sectional direction of the CLT slab were found important, and properties of the uppermost lamella seemed to

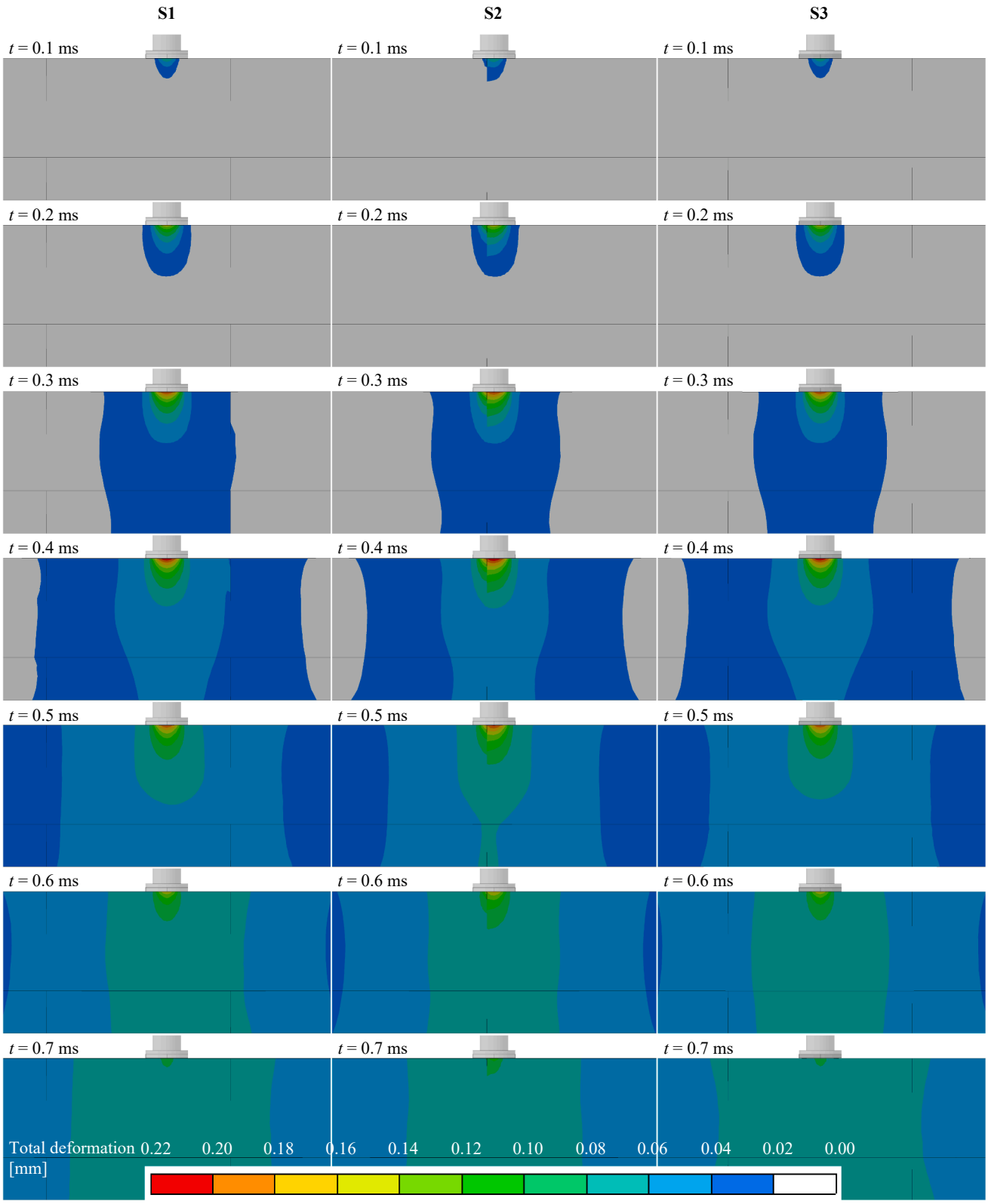

Fig. 11. Total (elastic) deformation process of the CLT slab during the impact at the source positions S1, S2, and S3.

affect the most significantly the impact force (Fig. 15). Furthermore, the force was slightly affected if the strength class of the centre lamella was changed, and major changes in the stiffness of the lower lamellae lead to greater influence on impact force. The former result also justifies the assumption of very thin and perfectly connecting glue layers between lamellae: if the thin glue layers would be modelled, probably the effect on the impact force would be minor, too. The most important material parameters for the impact force were found to be the modulus of elasticity E_R, the shear modulus G_{LR}, and the density ρ of the slab (Fig. 16). In the sensitivity analysis, the values of material parameters were varied one at a time. Thus, it is likely that the real material changes affect the impact force even more. Thirdly, the presence of the heartwood in the

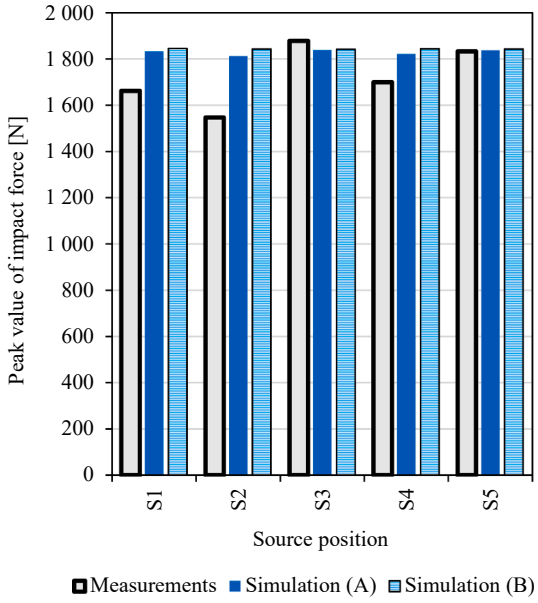

Fig. 12. Peak values of the force: comparison of the measurement and simulation results (slab configurations A and B).

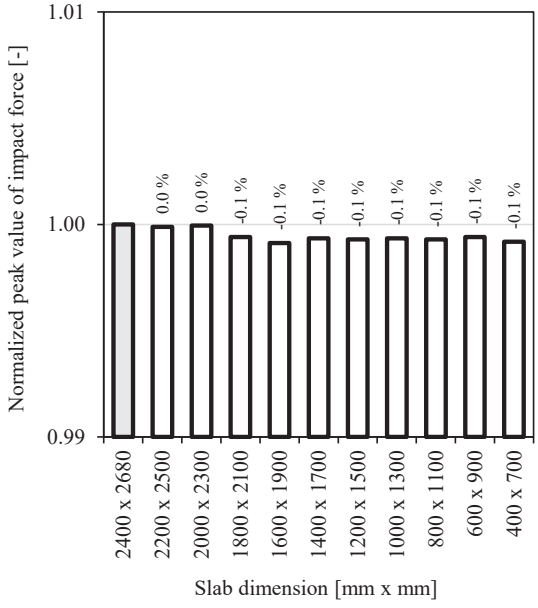

Fig. 13. Sensitivity of slab dimension on the peak value of the impact force (normalized to the result of the model in validation, in grey colour).

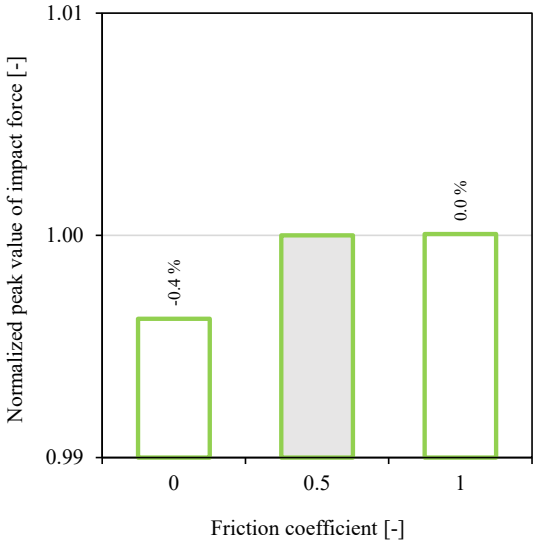

Fig. 14. Sensitivity of friction coefficients on the peak impact force (normalized to the result in grey colour).

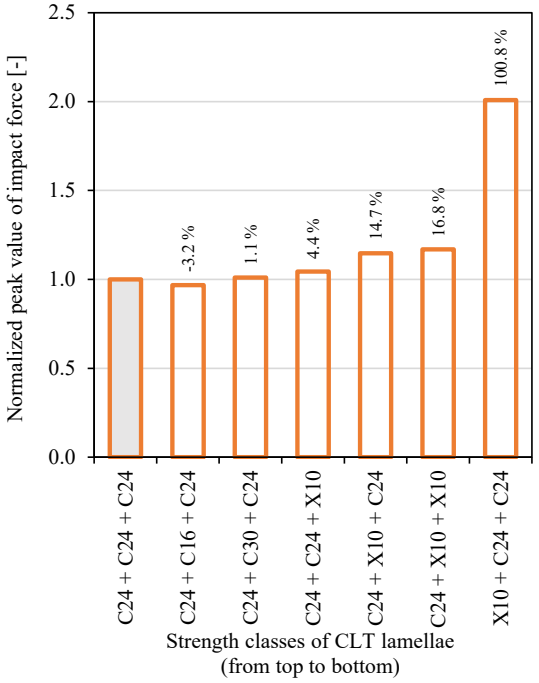

Fig. 15. Sensitivity of the lamellae's strength class on the peak impact force (normalized to the result in grey colour).

impacted part of the slab was found to be a significant feature explaining the differences in the force pulses at different distances from the board edges (Fig. 18). If the annual rings of wood are evident and the specimen is well known, the use of rotated cartesian (or cylindrical) coordinate system is justified for improving the computational accuracy.

The abovementioned findings indicate that the local properties of the CLT slab close to the impacted area are important to the impact force. However, the friction between the hammer and the slab did not affect the force (Fig. 14). This can be regarded important since exact friction coefficients between the hammer and the floors are not necessarily known. In addition, it was found that the impact force was insensitive to the global position of the hammer on the CLT slab (Fig. 12), and to the slab size or boundary conditions (Fig. 13), i.e., the global properties of the slab. These findings support modelling only a part of the slab around the impact area to still compute the impact force pulse accurately. This occurs because the stress waves caused by the impact to the slab cannot reach the impact area from the boundaries during the time of contact (Fig. 11).

The results of the sensitivity analysis imply possibilities to develop computational models for engineers and researchers. First, the need to model only a part of the impacted floor to reach accurate results provides a route to efficient tools for acoustical engineers' and researchers' purposes even when large structures are studied. Second, to compute the impact force results reaching for values on the safe side, i.e., close to the maximum, modelling the timber boards as linear orthotropic elastic material with principal axes in cartesian coordinate system and as continuous layers can offer a solution. For research purposes, it must be

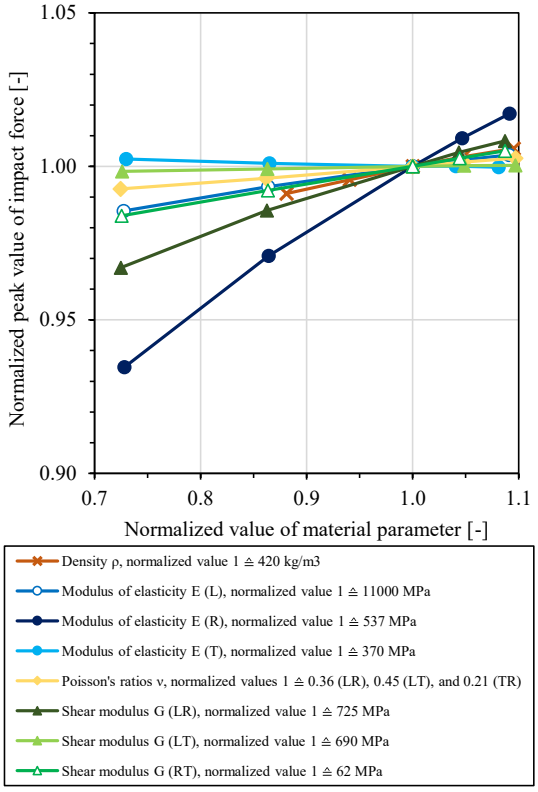

Fig. 16. Sensitivity of material parameters of the CLT slab on the peak impact force.

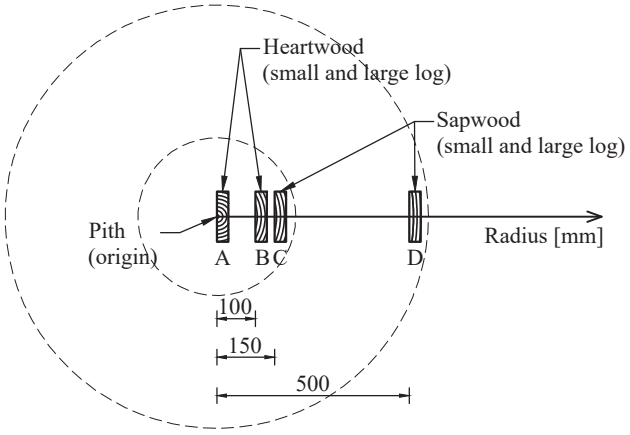

Fig. 17. Studied locally rotated coordinate systems.

noted that changes in material properties affect the results and lead to spatial variation even on CLT slabs. To take this into account, the slabs must be modelled in detail and accurate information from the material parameters is needed. If the presented techniques for modelling impact force pulses generated by the hammers of the STM are used to compute point forces driving the floor for ISI prediction models, the post-processing procedure can be implemented in simulation tools as illustrated in Section 2.1 and Fig. 19. Note that the findings from the sensitivity analysis should be verified case by case if other floors are studied with the presented procedure.

4.2. Limitations and need for further research

As with all models, it should be noted that the finite element model

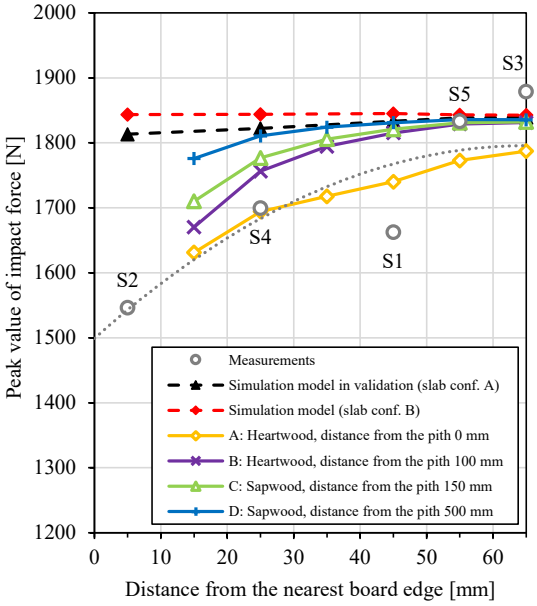

Fig. 18. Effect of the heartwood and sapwood on the peak impact force: comparison of measurement and simulation results. The average measurement results at different source positions have been indicated with labels S1–S5 and with a polynomial trend line of order two (dotted (:) grey line).

presented in this paper was used under a few assumptions. First, the CLT slab was initially at rest in the simulations. This initial state is based on the findings from the experimental study [10] as noted in Section 2.3.2. Because of this, the finite element model was used to compute the force pulse generated by a single hammer drop. It would be interesting if in further research the effect of the vibration of the slab on the impact force would be studied in detail with simulations. One possible way for this is to connect implicit finite element analysis describing the vibration behaviour of the slab to the impact force analysis. Secondly, the finite element model did not include material damping since the model was used to simulate only a very short collision between the bodies. For further studies, Rayleigh damping, especially the β damping factor (stiffness matrix damping multiplier), could be incorporated if the effect of the damping on the impact force is of interest. However, according to our knowledge and experience, damping would only minorly affect the impact force results shown in this paper. Thirdly, a regular contact-impact algorithm was used in the finite element model to simulate the collision between bodies. For engineering and research purposes, it would be interesting to study the possible benefits of using a SMOOTH option (surface fitting algorithm) [27] for the contact. The SMOOTH contact can provide a more accurate presentation of the curvature of the hammer head and produce smoother results with coarser meshes [27]. Thus, using SMOOTH contact could improve the mesh convergence.

5. Conclusions

This paper presented a method to simulate the impact force pulse generated by a hammer of the STM on a wooden slab by using explicit dynamics analysis. According to the model validation and sensitivity analysis, the method is applicable in computing the non-linear behaviour of the contact between the hammer and the slab. The validated model predicted closely the maximum impact force measured on the CLT slab both in time and frequency domains. Local properties of the CLT slab were discovered to be important to the results. The discrepancies between the simulation and the measurement results were suggested to be affected by the local material properties of the CLT slab: both material parameters and the use of heartwood explained the differences. On the other hand, the global properties such as the location of

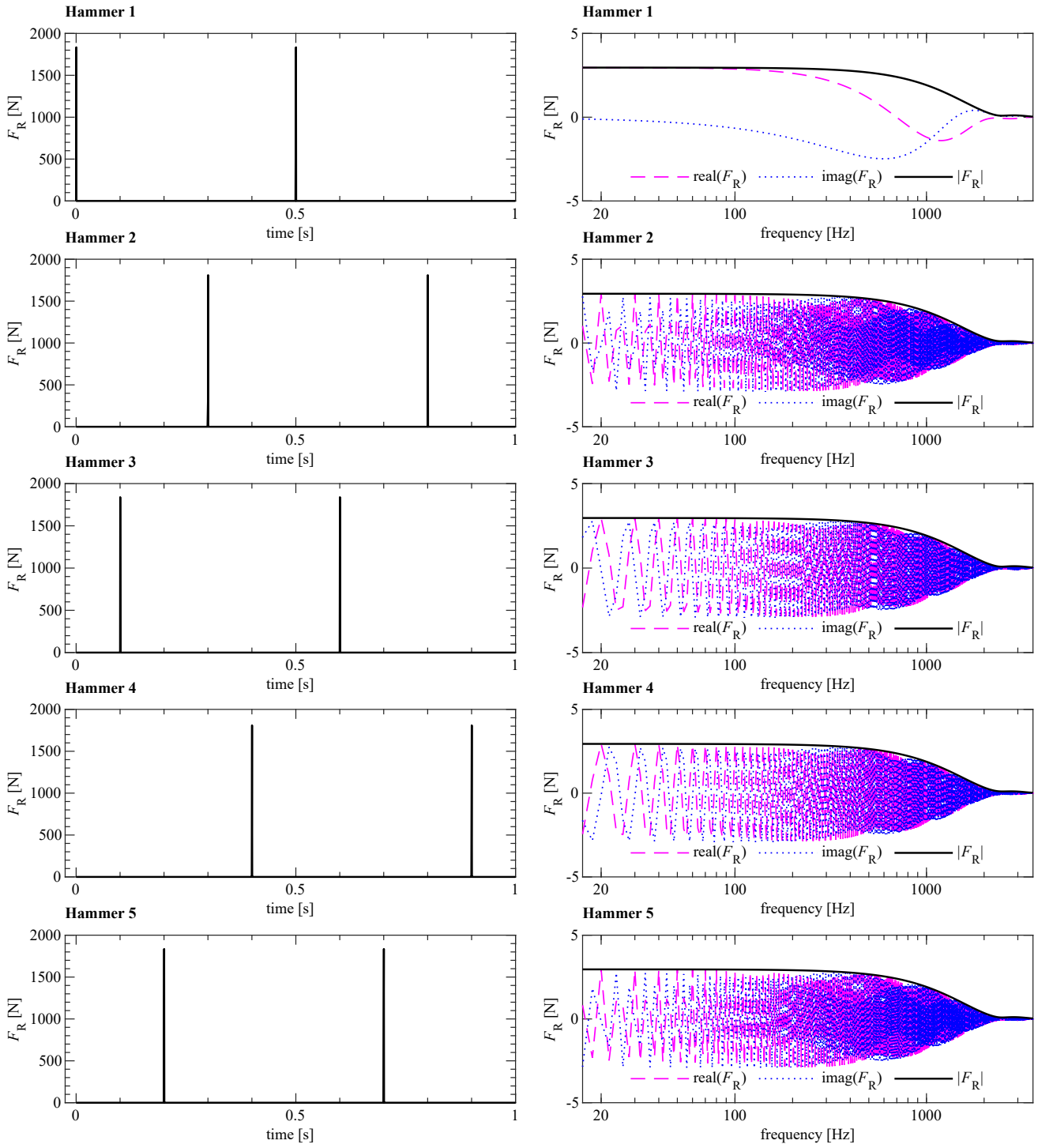

Fig. 19. Post-processed impact force results for time domain simulations (left), and for frequency domain simulations (right). For the frequency domain results, the magnitude (solid black line), the real part (dashed (–) magenta line), and the imaginary part (dotted (:) blue line) of the force spectrum $F_R(f)$ has been presented.

the hammer on the slab and the slab size were found to be insignificant to the simulated impact force pulses. The findings from the sensitivity analysis offer possibilities to develop tools predicting the excitation force for both engineering and research purposes. The post-processing procedure can be implemented in these tools to achieve point forces describing the continuous excitation generated by the STM in time and frequency domains.

The simulations were performed for a CLT slab, but the authors see no reason to restrict the use of the presented techniques to CLT or other massive wooden slabs only. The mathematical presentation of the model is valid on floor structures in general. Hence, the structures can include other types of wooden floors and, e.g., surface structures such as additional layers, floating floors, or floor coverings, if only their properties are known. However, there is a need for further sensitivity analyses when developing corresponding simulation models for other types of floors.

Declaration of Competing Interest

The authors declare that they have no known competing financial

interests or personal relationships that could have appeared to influence the work reported in this paper.

Acknowledgements

This paper was written within the Doctoral School in Industrial Timber Construction of Tampere University.

References

[1] Rabold A, Düster A, Rank E. FEM based prediction model for the impact sound level of floors. Proc Acoust '08 2008;123. https://doi.org/10.1121/1.2933931.
[2] Kohrmann M, Buchschmid M, Schanda U, Müller G. A FEM-based planning tool for the vibro-acoustic design of wooden floors at low frequencies. Proc. INTER-NOISE 2016 - 45th Int. Congr. Expo. Noise Control Eng. Towar. a Quieter Futur., Hamburg, Germany: 2016, p. 3743–51.
[3] Bard D, Negreira J, Guigou Carter C, Borello G, Kouyoumji J, Speranza A, et al. Modelling prerequisites – FEM/SEA Impact and Airborne Sound. Silent Timber Build, repor no STB01 WG1. 2017.
[4] Qian C, Ménard S, Bard-Hagberg D, Kouyoumji JL, Negreira J. Calibration of the ISO tapping machine for finite-element prediction tool on a wooden-base floor. Build Acoust 2019;26:157–67. https://doi.org/10.1177/1351010X19855227.
[5] Wang P, Van hoorickx C, Lombaert G, Reynders E. Numerical prediction and experimental validation of impact sound radiation by timber joist floors. Appl Acoust 2020;162:107182.
[6] ISO 10140-5. Acoustics – Laboratory measurement of sound insulation of building elements – Part 5: Requirements for test facilities and equipment. Geneva: International Organization for Standardization; 2010.
[7] Iso. 16283–2. Acoustics – Field measurement of sound insulation in buildings and of building elements – Part 2: Impact sound insulation. Geneve: International Organization for Standardization; 2015.
[8] Brunskog J, Hammer P. The interaction between the ISO tapping machine and lightweight floors. Acta Acust United with Acust 2003;89:296–308.
[9] Cremer L, Heckl M, Petersson BAT. Structure-Borne Sound. 3rd ed. Berlin Heidelberg: Springer-Verlag; 2005.
[10] Lietzén J, Miettinen J, Kylliäinen M, Pajunen S. Impact force excitation generated by an ISO tapping machine on wooden floors. Appl Acoust 2021;175:107821.
[11] Heckl M, Rathe EJ. Relationship between the transmission loss and the impact-noise isolation of floor structures. J Acoust Soc Am 1963;35:1825–30. https://doi.org/10.1121/1.1918830.
[12] Lindblad S. Impact sound characteristics of resilient floor coverings. Sweden: Lund; 1968.
[13] Vér IL. Impact noise isolation of composite floors. J Acoust Soc Am 1971;50:1043–50. https://doi.org/10.1121/1.1912726.
[14] Cremer L, Heckl M, Ungar EE. Structure-Borne Sound. Berlin Heidelberg: Springer-Verlag; 1973.
[15] Scholl W, Maysenhölder W. Impact sound insulation of timber floors: interaction between source, floor coverings and load bearing floor. Build Acoust 1999;6:43–61. https://doi.org/10.1260/1351010991501266.
[16] Griffin D. Accuracy of prediction methods for the improvement of impact sound pressure levels using floor coverings. Proc. Internoise 2017, Hong Kong, China: 2017, p. 3805–13.
[17] Rabold A, Buchschmid M, Düster A, Müller G, Rank E. Modelling the excitation force of a standard tapping machine on lightweight floor structures. Build Acoust 2010;17:175–97. https://doi.org/10.1260/1351-010X.17.3.175.
[18] Wittstock V. On the spectral shape of the sound generated by standard tapping machines. Acta Acust United with Acust 2012;98:301–8. https://doi.org/10.3813/AAA.918513.
[19] Amiryarahmadi N, Kropp W, Bard D, Larsson K. Time-domain model of a tapping machine. Proc. Forum Acusticum 2011, Aalborg, Denmark: 2011, p. 1713–8.
[20] Coguenanff C, Guigou-Carter C, Jean P, Desceliers C. Probabilistic model of the impact force spectrum for the standard ISO tapping machine. Proc. 22nd Int. Congr. Sound Vib. ICSV 2015, Florence, Italy: 2015, p. 5551–8.
[21] Mosharrof MS, Brunskog J, Ljunggren F, Ågren A. An improved prediction model for the impact sound level of lightweight floors: Introducing decoupled floor-ceiling and beam-plate moment. Acta Acust United with Acust 2011;97:254–65. https://doi.org/10.3813/AAA.918405.
[22] Rao CL, Narayanamurthy V, Simha KRY, editors. Applied Impact Mechanics. Chichester, UK: John Wiley & Sons, Ltd; 2016.
[23] Wu SR, Gu L, editors. Introduction to the Explicit Finite Element Method for Nonlinear Transient Dynamics. Wiley; 2012.
[24] ETA-14/0349. European Technical Assessment. Austrian Inst Constr Eng 2014.
[25] LS-DYNA Theory Manual. r:8571. Livermore, California: Livermore Software Technology Corporation (LSTC); 2017.
[26] Wu SR. Lumped mass matrix in explicit finite element method for transient dynamics of elasticity. Comput Methods Appl Mech Eng 2006;195:5983–94. https://doi.org/10.1016/j.cma.2005.10.008.
[27] LS-DYNA Keyword User's Manual, Volume I (r:8752). Livermore, California: Livermore Software Technology Corporation (LSTC); 2017.
[28] LS-DYNA Keyword User's Manual, Volume II: Material Models (r:8944). Livermore, California: Livermore Software Technology Corporation (LSTC); 2017.
[29] EN 1993-1-1. Eurocode 3: Design of steel structures - Part 1-1: General rules and rules for buildings. Brussels: European Committee for Standardization; 2005.
[30] EN 1993-1-4. Eurocode 3: Design of steel structures - Part 1-4: General rules - Supplementary rules for stainless steels. Brussels: European Committee for Standardization; 2006.
[31] Wood Handbook – Wood as an Engineering Material. Madison, Wisconsin: U.S. Department of Agriculture, Forest Service, Forest Products Laboratory; 2010.
[32] EN 338. Structural timber – Strength classes. Brussels: 2016.
[33] Keunecke D, Hering S, Niemz P. Three-dimensional elastic behaviour of common yew and Norway spruce. Wood Sci Technol 2008;42:633–47. https://doi.org/10.1007/s00226-008-0192-7.